

High-temperature elasticity of polycrystalline orthoenstatite (MgSiO₃)

JENNIFER KUNG,^{1,2,*} IAN JACKSON,³ AND ROBERT C. LIEBERMANN²

¹Department of Earth Sciences, National Cheng Kung University, Tainan 70101 Taiwan

²Mineral Physics Institute and Department of Geosciences, Stony Brook University, New York 11794-2100, U.S.A.

³Research School of Earth Sciences, The Australian National University, Canberra, ACT 0200, Australia

ABSTRACT

Compressional and shear wave velocities of a polycrystalline specimen of MgSiO₃ orthoenstatite have been measured by ultrasonic interferometry to 1373 K at 300 MPa in an internally heated gas-medium apparatus. The elastic wave velocities and bulk and shear moduli vary linearly with temperature to 1073 K. Below 1073 K, the temperature derivatives of the elastic moduli [$(\partial K_s/\partial T)_p = -28.3(7)$ MPa/K and $(\partial G/\partial T)_p = -14.5(1)$ MPa/K, respectively] determined in this study are consistent with averages of single-crystal elastic constants measured using Brillouin spectroscopy by Jackson et al. (2007). The measured temperature dependence of elastic moduli, along with pressure dependence of elastic moduli, thermal expansion and calorimetric data have been assimilated into a finite-strain equation of state of the type proposed by Stixrude and Lithgow-Bertelloni (2005). This analysis suggests significant revisions to the optimal values of the zero-pressure Grüneisen parameter γ_0 and its zero-pressure logarithmic volume derivative q_0 . The unusually high absolute values of $(\partial K/\partial P)_T$ and $(\partial K/\partial T)_p$ are related through the extrinsic part of the temperature derivative. Above 1073 K, a pronounced softening of the elastic wave velocities is observed, which is plausibly associated with a phase transformation for which there is microstructural evidence: The recovered specimen was found to have transformed to the low-pressure clinoenstatite polymorph.

Keywords: MgSiO₃ orthoenstatite, elasticity, high temperature, elastic velocity softening, phase transition

INTRODUCTION

To interpret seismological models of the Earth's mantle, we need to know the elastic properties of the candidate mineral phases. From field evidence (e.g., McDonough and Rudnick 1998), the pyroxenes (Ca-poor and -rich), olivine, and garnet are suggested to be the major phases of the upper mantle. In the upper mantle, orthoenstatite, i.e., Ca-poor pyroxene, is thought to be an important phase in the harzburgite or the "depleted" mantle composition (Jordan 1978), which may present an average chemical composition for continental lithosphere. The enstatite component often exhibits an orthorhombic symmetry (space group *Pbca*, orthoenstatite, OEN) in the mantle specimens, for which the dominant end-members are represented in the formula (Mg,Fe)SiO₃.

Both the Mg-end-member (MgSiO₃) and (Mg,Fe)SiO₃ compositions have been widely investigated for their elastic properties (Frisillo and Barsch 1972; Ito et al. 1977; Webb and Jackson 1993; Flesch et al. 1998; Angel and Jackson 2002; Jackson et al. 2003, 2004, 2007). A key finding from such ultrasonic and X-ray diffraction studies has been the unusually high initial pressure derivative (8–11) of the bulk modulus. Kung et al. (2004) extended the experimental conditions to higher pressures and found that there is a velocity anomaly in MgSiO₃ near 12 GPa. The velocity softening behavior was attributed to a phase transition to a high-pressure polymorph (space group

P2₁ca) with a displacive relationship to *Pbca* (Jahn 2008). A similar observation was made by Jackson et al. (2004) at high temperature (to 1400 K); P and S wave velocities along different crystallographic directions presented strong non-linear behavior at high-temperature regime (above 1000 K). From the MgSiO₃ phase diagram (e.g., Gasparik 1990), the maximum temperature in the study of Jackson et al. (2004) should approach that of the high-temperature phase transformation. It has long been known that MgSiO₃ orthoenstatite transforms into an unquenchable high-temperature phase for which the crystal structure is still in dispute—protoenstatite with orthorhombic symmetry and space group *Pbcn* or high-temperature clinoenstatite with monoclinic symmetry and space group *C2/c* being observed in most studies (e.g., Smyth 1974; Murakami et al. 1982; Shimobayashi and Kitamura 1993; Yang and Ghose 1995; Ohi et al. 2010). The transition temperature revealed by various studies spans a wide range (reviewed by Jackson et al. 2004, references therein). The single-crystal Brillouin scattering measurements (Jackson et al. 2004, 2007) have provided the temperature derivatives of aggregate properties of orthoenstatite up to 1073 K and selected elastic moduli to 1400 K at ambient pressure.

Recent improvements to the experimental technique for high-temperature MHz ultrasonic interferometry allow measurement up to 1600 K at a confining pressure of 300 MPa (Jackson et al. 2005). The advantage of this technique is access to the aggregate properties by measuring an elastically isotropic polycrystalline specimen—providing ready experimental access to any

* E-mail: jkung@mail.ncku.edu.tw

anomalies in compressional and shear wave velocities across the temperature-induced phase transition. In this study, we use the MHz ultrasonic technique to revisit the elasticity of MgSiO₃ orthoenstatite up to temperature near 1400 K. By combining current results with previous measurements, we reassess the thermoelastic properties of MgSiO₃ orthoenstatite.

EXPERIMENTAL PROCEDURES

Specimen synthesis

Polycrystalline specimens of MgSiO₃-orthoenstatite (OEN) were synthesized from glass at 5 GPa, ~1300 K (well within the orthoenstatite stability field) in a uniaxial split-sphere apparatus in the Stony Brook High Pressure Laboratory. The synthesized specimen had an average grain size of less than 10 μm and was about ~2.8 mm in diameter and ~2.84 mm long with a bulk density within 1% of the single-crystal value; the X-ray density was used to calculate the elastic moduli from the measured velocities. The same polycrystalline specimen was used to perform two high-temperature ultrasonic measurements.

Ultrasonic interferometry experiments

High-temperature ultrasonic measurements were carried out in an internally heated gas-medium high-pressure apparatus to temperature of 1573 K under pressures of 300 MPa at the Research School of Earth Sciences, Australian National University. The incorporation of a dual-mode transducer (LiNbO₃, 10° rotated Y-cut), which generates both P and S elastic waves at the same time, enables simultaneous measurement of travel times of P and S waves, thereby avoiding the necessity of combining data sets from separate experiments with pure-mode transducers (Jackson et al. 2005). The current experiments were carried out using the latest acoustic cell assembly described in Jackson et al. (2005). In brief, measurement of two-way travel times was performed with the phase comparison method using an Australian Scientific Instruments interferometer (Jackson and Niesler 1982; Niesler and Jackson 1989; Jackson et al. 2005). Travel time through the specimen was determined from superposition of buffer rod echo and specimen echo resulting in a series of successive interference extreme across a wide range of carrier frequency. Thin foils of Au (1 μm thick) and Fe (1 μm thick) were used at the interfaces between the various parts of acoustic path to provide optimal mechanical coupling (Fig. 1). The measured travel times have been corrected for the influence of the foil inserted between buffer-rod and specimen and the “cup” enclosing the specimen (Fig. 1). A tapered Al₂O₃ buffer rod shown in Figure 1 was employed here to optimize the relative amplitudes of the echoes resulting from partial reflection at the near and far ends of the specimen (detailed discussion in Jackson et al. 2005). In this study, NaCl (melting temperature ~1073 K) and Fe (melting temperature ~1811 K) were chosen as cup materials providing quasi-hydrostatic conditions; the former was used in lower temperature run (run5745) and the latter in higher temperature run (run5748).

Data collection

Two ultrasonic experimental runs to temperatures up to 973 K (run 5745) and 1573 K (run 5748), respectively, were performed at 300 MPa argon confining

pressure; this modest confining pressure, acting across the buffer rod-foil boundary, helps to improve the mechanical coupling between the interfaces in the acoustic assembly. In this study, three heating cycles were carried out in each run. In the run 5745, NaCl was used as confining medium and gold foil was inserted between Al₂O₃ buffer rod and specimen. In the other run (run 5748), iron was used as both the confining medium and foil insert. During the experiments, it was found that the mechanical contact across the metal foils embedded within the acoustic path (Fig. 1) was not optimized until the temperature reached at least 800 K under the confining pressure of 300 MPa along the first heating path (see also Jackson et al. 2005). Due to the imperfect mechanical coupling across the metal foils during the first heating cycle, the data collected in this cycle of each run reported here have been discarded in our analysis. Consequently, most of our acoustic measurements were made during subsequent slow cooling under confining pressure of 300 MPa from the peak temperature to room temperature.

In run 5748, the data for the third heating cycle were collected as the temperature increased from 1128 K to 1573 K instead of during cooling, because the mechanical coupling had been well established during the previous two thermal cycles.

The amplitudes of the echoes from the buffer rod and sample were also monitored (Fig. 2, shown as buffer rod/specimen ratio) during the course of the experimental runs. During the third heating cycle from 1128 K to 1573 K in run 5748, the amplitudes for P and S wave signals started decreasing above 1323 K and disappeared entirely beyond 1423 K. Due to high buffer rod/specimen ratio above temperature of 1323 K, the travel times for P and S waves were not measured at temperatures beyond 1373 and 1323 K, respectively. The specimen was recovered from 1573 K, 300 MPa to ambient conditions (within 7–8 h), and examined by light microscopy and X-ray diffraction at X17B2 beamline of National Synchrotron Light Source (NSLS) of the Brookhaven National Laboratory.

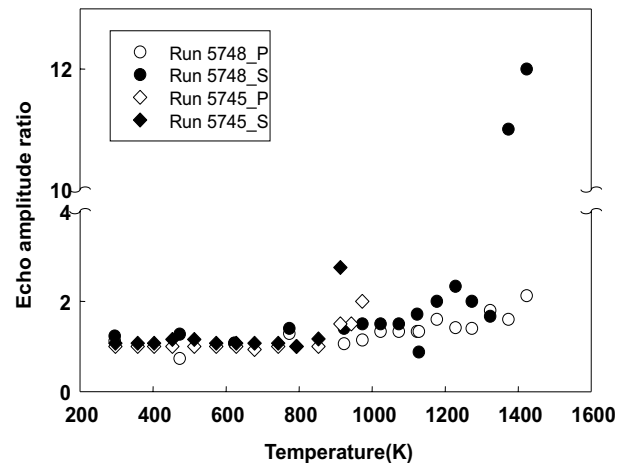


FIGURE 2. The temperature dependence of the echo amplitude ratio (buffer/sample).

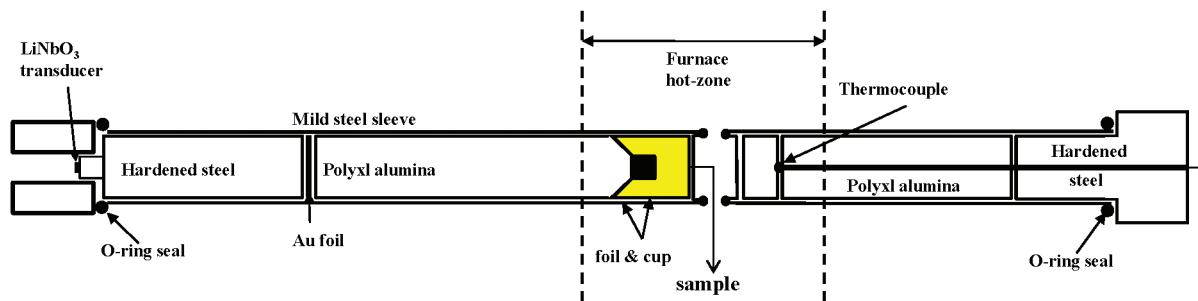


FIGURE 1. Cross-sections of the experimental assembly employed in measurements of temperature dependence of travel time within an internally heated gas-loaded pressure apparatus. The materials used for the metallic foils and cups vary with the experimental conditions, as described in the text.

EXPERIMENTAL RESULTS

The travel times were determined within a broad range of carrier frequency, 20–55 MHz for P wave and 20–38 MHz for S wave. A series of selected P wave travel time is plotted against frequency in Figure 3 for temperatures from 293 to 1373 K from run 5748; these travel times are essentially frequency independent over a wide range of frequencies. The somewhat scattered travel times in the narrow range 35–38 MHz probably result from subsidiary echoes arising from complications in the acoustic path (Jackson et al. 2005). The preferred value of the travel time at each temperature was averaged from 38–55 MHz for P wave, 28–36 MHz for S wave. The standard errors in the averaged travel times were less than 0.4% for P wave (travel time from 0.70–0.80 μ s) and 0.3% for S wave (travel time from 1.16–1.30 μ s), respectively.

To calculate the velocities from the travel time data, the specimen length at each experimental condition is essential. In the absence of in situ length measurement during the course of experiment, the specimen lengths at experimental condition were calculated using the thermal expansion data for MgSiO₃ orthoenstatite from Jackson et al. (2003). Similar velocities (within 0.1%) were obtained with alternative thermal expansion data (Yang and Ghose 1994; Hugh-Jones 1997). As a result, the variation in velocities derived from above thermal expansion data is less than 0.3% at high temperature. The resulting wavespeeds and elastic moduli (Figs. 4 and 5) are discussed below in two different temperature regimes; below 1073 K and above 1073 K.

Below 1073 K

As illustrated in Figure 4 and summarized in Table 1, both the P and S wave velocities derived from travel time measurements (Fig. 3) and calculated length decrease smoothly as temperature increases. Below 1073 K, the velocities collected during the three cooling cycles in the two different runs (run 5745 and 5748) agree within experimental uncertainty and define an approximately linear trend (see gray solid lines in Fig. 4). Our velocity data are also in excellent agreement with those calculated from the recent single-crystal data obtained over the same temperature range (Table 2 and Fig. 4).

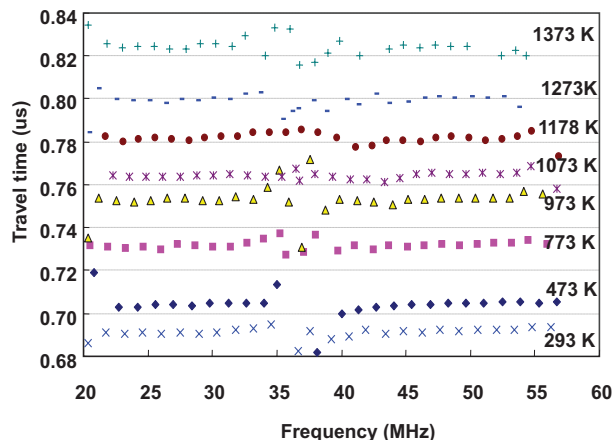


FIGURE 3. Selected P wave travel times for polycrystalline MgSiO₃ orthoenstatite as a function of temperature.

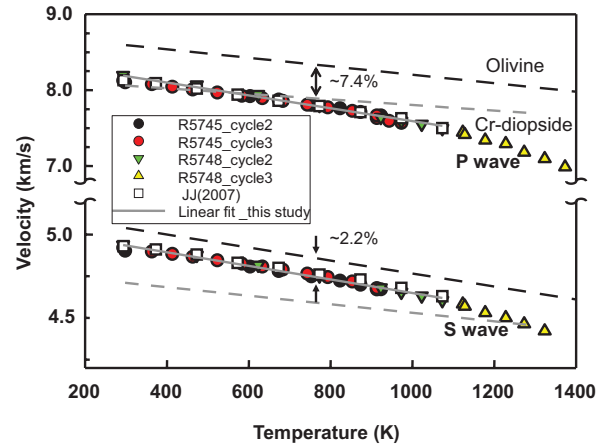


FIGURE 4. Derived P and S wave velocities of orthoenstatite (circles and triangles from this study; squares from Jackson et al. 2007), olivine (black dashed line, Isaak et al. 1989) and diopside (gray dashed line, Isaak et al. 2006) plotted as functions of temperature. The P and S wave velocities depart from linear temperature dependence above 1073 K.

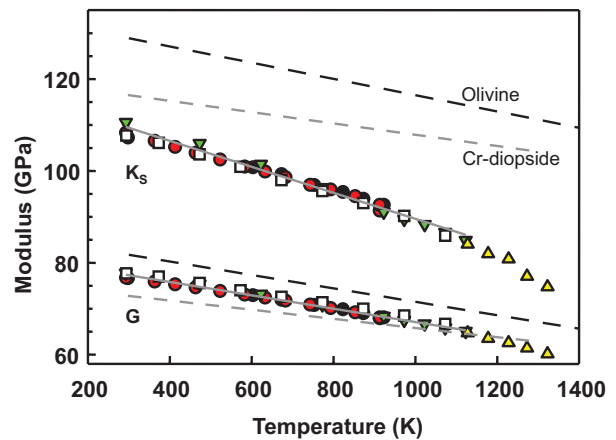


FIGURE 5. Derived K_s and G moduli of orthoenstatite, olivine, and diopside plotted as functions of temperature. Elastic moduli of orthoenstatite show strong curvature above 1073 K. Symbols shown in this figure are the same as those in Figure 4.

Due to the similarity among the velocity data sets in our study, we chose to fit all the data collected in different runs below 1073 K. The average linear temperature derivatives of velocity are $-8.5(2) \times 10^{-4}$ and $-4.1(1) \times 10^{-4}$ km/s/K for P and S waves, respectively, and the resultant average temperature derivatives of the elastic moduli are $(\partial K_s / \partial T)_p = -28.3(7)$ and $(\partial G / \partial T)_p = -14.5(1)$ MPa/K. These derivatives agree with those derived from the single-crystal data of Jackson et al. (2007) in the same temperature range.

Above 1073 K

To achieve higher temperatures in our experiments, an iron backing cup was used as the confining material in run 5748. In the third thermal cycle of run 5748, the data were collected as the temperature was increasing. During this heating cycle, the

TABLE 1. Elastic velocities of polycrystalline MgSiO₃ orthoenstatite at high temperature, 300 MPa

	Temperature (K)	V _P (km/s)	V _S (km/s)	
Run 5745 (NaCl cup)				
Cycle 2	973	7.60(1)		
	923	7.67(3)	4.67(1)	
	873	7.71(3)	4.70(1)	
	823	7.76(2)	4.72(1)	
	753	7.81(2)	4.75(1)	
	673	7.87(2)	4.78(1)	
Cycle 3	603	7.92(2)	4.81(1)	
	298	8.10(3)	4.90(1)	
	973	7.57(1)		
	943	7.59(3)		
	913	7.63(2)	4.66(1)	
	853	7.73(3)	4.70(1)	
	793	7.77(2)	4.73(1)	
	743	7.81(3)	4.75(1)	
	683	7.86(3)	4.77(1)	
	633	7.89(2)	4.79(1)	
	583	7.92(2)	4.81(1)	
	523	7.97(2)	4.83(1)	
	463	8.01(3)	4.85(1)	
	413	8.04(3)	4.87(1)	
363	8.08(3)	4.88(1)		
293	8.13(2)	4.91(1)		
Run 5748 (Fe cup)				
Cycle 2	1123	7.44(2)	4.58(1)	
	1073	7.49(3)	4.60(1)	
	1023	7.55(1)	4.63(1)	
	973	7.59(2)	4.65(1)	
	923	7.64(1)	4.68(1)	
	773	7.80(1)	4.75(1)	
	623	7.94(1)	4.82(1)	
	473	8.07(1)	4.88(1)	
	293	8.19(1)	4.94(1)	
	Cycle 3	1128	7.41(2)	4.57(1)
		1178	7.34(2)	4.53(1)
1228		7.29(2)	4.50(1)	
1273		7.18(2)	4.46(1)	
1323		7.09(2)	4.42(1)	
1373		6.89(2)		

TABLE 2. High-temperature elastic properties of MgSiO₃ enstatite and major mantle phases

	Velocity		$\partial V/\partial T (\times 10^{-4})$		$\partial M/\partial T$	
	P	S	P	S	K _s	G
	T = 295 K					
	km/s	km/s	km/s/K	km/s/K	MPa/K	MPa/K
Run 5745	8.03	4.88	-8.1(2)	-4.0(1)	-25.0(1)	-13.9(1)
Run 5748	8.03	4.90	-9.2(3)	-4.3(1)	-32.0(5)	-15.5(1)
Averaged			-8.5(2)	-4.1(1)	-28.3(7)	-14.5(1)
JJ (2006)			-7.53(8)	-3.62(5)	-26.3(3)	-13.6(3)
HP-CEN			-5.0	-3.0	-17	-15
Diopside			-3.66	-2.56	-12.3	-10.0
Olivine			-5.5	-3.9	-17.6	-14.5

Notes: Averaged values; the derivatives were fitted using the data points from both runs. JJ (2007): Single-crystal Brillouin scattering, Jackson et al. (2007). HP-CEN: MgSiO₃ high-pressure enstatite with space group C2/c, Kung et al. (2005). The values presented here were at conditions of 6.5 GPa, due to it is a unquenchable phase. Olivine: Isaak et al. (1989). Diopside: Cr-bearing diopside, Isaak et al. (2006).

acoustic signal from the specimen retained good amplitude until the temperature approached 1323 K, above which the sample echo started to decrease in amplitude (Fig. 2). This is especially pronounced for S waves, as reflected in the dramatic increase in the ratio of buffer rod/specimen echo amplitudes illustrated in Figure 2. Above this temperature (1473 K), the specimen signals for both P and S waves disappeared and did not return during subsequent cooling. Therefore, the elastic velocities for P and

S wave were reported up to 1373 and 1323 K (Table 1 and Fig. 4), respectively, and the resulted elastic moduli were shown up to 1323 K in Figure 5.

As shown in Figure 4, the trends of P and S wave velocities for the orthoenstatite phase in this study clearly depart from linearity above 1073 K. Such behavior of elastic properties is unusual for silicate minerals at high temperature; by contrast, velocities for other upper mantle phases, olivine and diopside, decrease linearly as functions of temperature (see black and gray dashed lines in Fig. 4 calculated from the data of Isaak et al. 1989, 2006). Jackson et al. (2005) have measured the wave velocities in a polycrystalline olivine specimen up to 1573 K in the same apparatus used in this study and also observed a linear trend with temperature. Therefore, the non-linear behavior observed in this study above 1073 K is most likely due to intrinsic changes in MgSiO₃-enstatite.

Previous studies have shown that MgSiO₃-orthoenstatite (space group *Pbca*) undergoes a temperature-induced phase transition near or above 1373 K to a high-temperature polymorph. The symmetry and space group of this high-temperature phase remains in dispute due to its unquenchable nature; some studies reported it as protoenstatite, orthorhombic symmetry and space group *Pbcn* (e.g., Smyth 1974; Murakami et al. 1982; Yang and Ghose 1995; Ohi et al. 2010) while others indicated it to be clinoenstatite with space group *C2/c* (e.g., Shimobayashi and Kitamura 1993). The recovered products for the high-temperature phase of MgSiO₃ enstatite at ambient conditions were orthoenstatite or low-pressure clinoenstatite (space group *P2₁/c*) depending on the cooling history (Brown and Smith 1963; Smyth 1974; Lee and Heuer 1987; Schrader et al. 1990).

The specimen recovered after heating to 1573 K in cycle 3 of run 5748 was found to be coarse grained and heavily fractured. Examination of this recovered specimen by light microscopy (courtesy of J. Fitz Gerald at the ANU) revealed the presence of pervasive twinning (Fig. 6) and an enhanced grain size ≥ 50 μm . We interpret this texture to indicate that the orthoenstatite specimen underwent grain growth during heating to more than 273 K above its synthesis temperature, transformation to a high-temperature phase, and then back-transformation to low-pressure clinoenstatite on cooling (indicated by the following post-mortem X-ray examination). X-ray diffraction patterns were taken from the recovered specimen in the energy dispersive mode at the X17B2 beamline of National Synchrotron Light Source of the Brookhaven National Laboratory (courtesy of L. Wang); these diffraction patterns were fitted using the General Structure Analysis System program (GSAS, Larson and Von Dreele 1988) based on models for MgSiO₃-orthoenstatite (OEN, space group *Pbca*) (Ghose et al. 1986) and low-pressure clinoenstatite (LP-CEN, space group *P2₁/c*) (Ohashi 1984). The refinements were started in the Rietveld mode. Final values of lattice parameter were obtained by a Le Bail refinement (Le Bail et al. 1988). From this analysis, we could identify LP-CEN unambiguously (Fig. 7b), with little or no evidence for residual OEN (cf. Fig. 7a taken from the starting phase). As the LP-CEN phase could result only from back-transformation of a high-temperature polymorph stable at higher temperature than OEN, the X-ray data support the conclusion of the light microscopy that the specimen transformed to a high-temperature polymorph at high temperature.

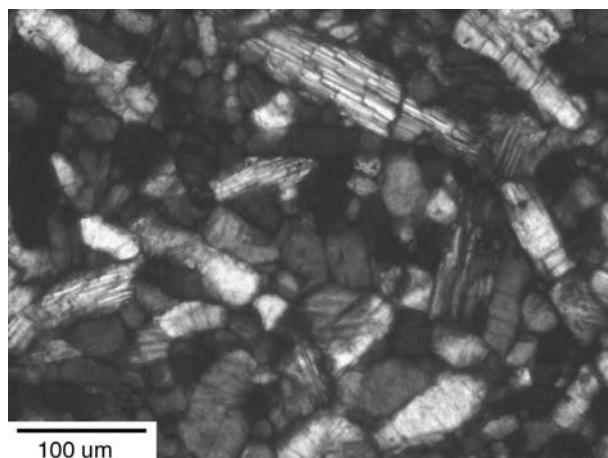


FIGURE 6. Transmitted light micrograph of the specimen recovered from the peak experimental conditions of 1573 K, 300 MPa, revealing grain growth to an average grain size $>50\ \mu\text{m}$ and length-parallel twin domains in many of the larger grains consistent with transformation at high temperature and recovery as low clinoenstatite (Fig. 7).

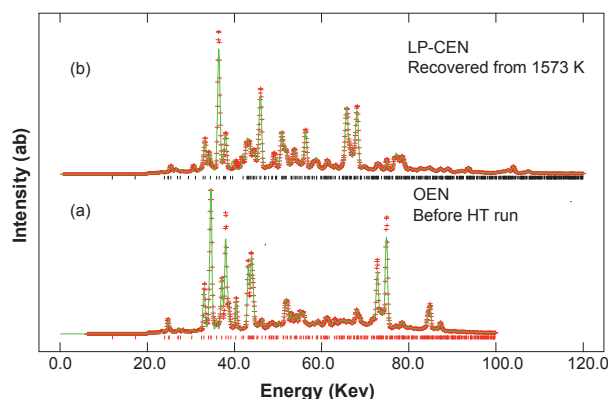


FIGURE 7. X-ray diffraction patterns for the orthoenstatite phase (a) and for the specimen studied here recovered from experimental conditions at 300 MPa, 1573 K (b), which was identified to be low-pressure clinoenstatite. The red crosses and green line represent the observed and calculated spectra, respectively. Black and red ticks represent the calculated peak positions of LP-CEN and OEN, respectively. Color online

DISCUSSION

High-*T* elasticity of MgSiO₃ orthoenstatite

In this study, the elastic properties of polycrystalline orthoenstatite have been measured using ultrasonic interferometry to temperature of 1373 K at 300 MPa in a gas-medium apparatus. The measured P and S wave velocities exhibit linear temperature dependence below 1073 K; as illustrated in Figure 4 of this study, our data are strikingly consistent with those derived from the recent single-crystal Brillouin scattering data over the same temperature range at ambient pressure (from Fig. 5 of Jackson et al. 2007) (compared in Figs. 4 and 5). The temperature derivatives of the elastic properties of MgSiO₃-orthoenstatite derived

from the data below 1073 K from this study agree well with those determined by Jackson et al. (2007) (Table 2) within mutual uncertainty. Comparison of the results of this study on a well-sintered polycrystalline specimen using ultrasonic interferometry with those of Jackson et al. (2007) study on a single-crystal specimen using Brillouin spectroscopy clearly demonstrates that mutually consistent results may be obtained at elevated temperature on the elasticity of mantle minerals.

Velocity softening at high temperature

Above 1073 K, the velocity-temperature trends for MgSiO₃ orthoenstatite exhibit significant deviation from linearity, accompanied by an anomalous behavior in signal as the temperature approaches 1373 K (Fig. 2). The velocity anomaly observed in this study (Fig. 4) is similar to that observed by Jackson et al. (2004) who attributed this behavior to elastic velocity softening ahead of a displacive phase transition preempted by the reconstructive phase transition. From our post mortem examination, the specimen was inferred to have transformed to a high-temperature phase and back-transformed to low-clinoenstatite based on the results from previous studies (Brown and Smith 1963; Smyth 1974; Lee and Heuer 1987; Schrader et al. 1990) but it is difficult to identify the transition temperature. The onset of softening in this study suggests a transition temperature above 1373 K, which is in accord with the observation of Jackson et al. (2004). A recent high-temperature Raman study of MgSiO₃ enstatite (Zucker and Shim 2009) reported the phase transition near 1500 K, but also showed premonitory softening of some of the low-frequency modes interpreted to reflect the reorganization of structure of Mg atoms and unkinking of the SiO₃ chains. Therefore, the observed elastic softening may be related to intrinsic softening of the structure prior the phase transition.

The acoustic data reported in this study are from measurements on a polycrystalline specimen, which are consistent with averages of single-crystal data from the literature up to 1073 K (Jackson et al. 2007). The velocity and moduli data reported in Figures 4 and 5 for this temperature interval are regarded as representative of the high-temperature behavior of an isotropic aggregate of MgSiO₃-orthoenstatite. In this study, we also compared the velocity data above 1073 K measured in this study and selected single-crystal moduli C_{ij} measured by Jackson et al. (2004), C_{33} (P wave along [001]) and C_{55} (S wave propagating along [001] with [100] polarization) using Brillouin spectroscopy (Fig. 8). Interestingly, we see that in the velocity softening regime, the isotropic S wave velocities are very similar to those determined from C_{55} (open symbols) by Jackson et al. (2004). But for the P wave data, the reduction in velocity measured on the polycrystalline specimen is much less pronounced above 1200 K than that determined from C_{33} (open symbols) in the single-crystal study. With these data, we are able to illustrate the v_p/v_s ratio as a function of temperature from 300 to 1400 K for aggregate MgSiO₃ orthoenstatite (full symbols, Fig. 9). The v_p/v_s ratio (related to Poisson's ratio, $\sigma = 0.5 \{1 - 1/[(v_p/v_s)^2 - 1]\}$) from the velocity measurements for the isotropic aggregate varies only mildly over this temperature range (from the value of 1.66 to 1.60), whereas the v_p/v_s ratio in the [001] direction from the single-crystal data, dramatically decreases from 1.65 to 1.35 above 800 K (see also Fig. 7 in Jackson et al. 2007).

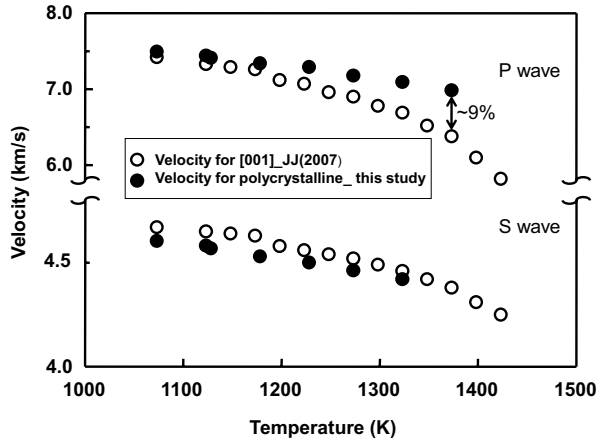


FIGURE 8. Comparison of elastic wave velocities measured from single crystal along [001] (Jackson et al. 2007) and from polycrystalline specimen (this study) as functions of temperature.

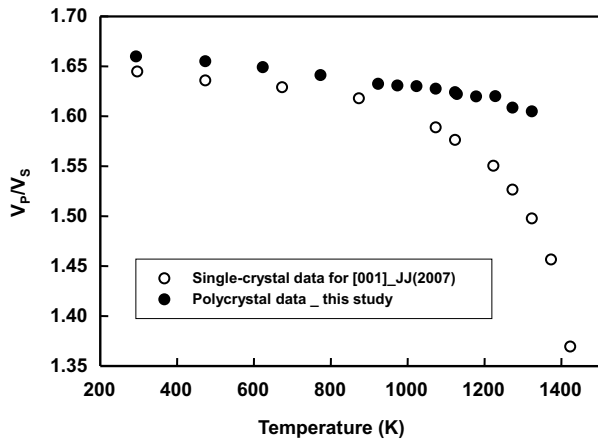


FIGURE 9. Comparison of the ratio of compressional wave velocity and shear wave velocity (v_p/v_s) along [001] (with [100] shear wave polarization) from single-crystal study (Jackson et al. 2007) and for polycrystalline specimen (this study).

TABLE 3. Details of the fits of the Stixrude-Lithgow-Bertelloni (2005) model to individual datasets for orthopyroxene of composition $Mg_2Si_2O_6^*$ except where otherwise specified

	K_{T0} (GPa)	G_0 (GPa)	K'_{T0}	G'_0	q_0 (K)	γ_0	q_0	η_{S0}	N	$\sqrt{\chi^2/N}$
SLB†	107(2)	77(1)	7.1(4)	1.6(1)	810(8)	0.67(4)	7.8(11)	2.4(5)		
Xu et al.‡	107(2)	77(1)	7.0(4)	1.5(1)	812(8)	0.78(4)	3.4(4)	2.5(1)		
$S(T)$ §	107.5	77.1	7.68	1.64	796(2)	0.94	1.87	2.31	8	3.62
$S(T)$	107.5	77.1	7.68	1.64	813(7)	0.94	1.87	2.31	1	0
K&G(P)#	109.5(1)	75.3(1)	8.83(4)	1.98(2)	813	0.94	1.87	2.31	26	3.14
K&G(P)**	106.4(7)	75.0(5)	7.68(21)	1.64(11)	813	0.94	1.87	2.31	22	0.86
K&G(P)††	105.0(10)	75.6(7)	8.02(30)	2.11(16)	813	0.94	1.87	2.31	12	0.99
$V(T,P)$ ‡‡	107.5	77.1	7.68	1.64	813	0.94(1)	1.87	2.31	85	1.83
G&L(T)§§	107.5(7)	77.1(2)	7.68	1.64	813	0.94	1.87(35)	2.31(14)	74	0.55
G&L(T)	107.5(7)	77.1(2)	8.02	2.11	813	0.94	1.55(34)	1.84(14)	74	0.55
Preferred	107(1)	77(1)	7.7(2)	1.6(1)	813(7)	0.94(1)	1.9(4)	2.3(1)		

* $V_0 = 62.676 \text{ cm}^3$, $n = 10$, $Z = 8$.

† Model of Stixrude and Lithgow-Bertelloni (2005).

‡ Model of Xu et al. (2008).

§ $S(T)$ for $300 \leq T \leq 1000 \text{ K}$ (Robie et al. 1995); $\sigma(S)/S = 0.005$.

|| Preferred fit (to $S(1000 \text{ K})$ only cf. Stixrude and Lithgow-Bertelloni 2005).

K_0 and G from $C_{ij}(P)$ $0 \leq P \leq 3 \text{ GPa}$ with $\sigma(M)/M = 0.001$ (liquid-medium ultrasonic interferometry for En_{80} by Webb and Jackson 1993).

** K_0 and G from solid-medium ultrasonic measurements of v_p and v_s (Flesch et al. 1998; Kung et al. 2004) for $P < 8 \text{ GPa}$ excluding data from run T354 of Kung et al. (2004); $\sigma(M)/M = 0.01$.

†† K_0 and G from solid-medium ultrasonic measurements of v_p and v_s for $P < 8 \text{ GPa}$ from run T354 only of Kung et al. (2004); $\sigma(M)/M = 0.01$.

‡‡ Data of Hugh-Jones (1997), Jackson (2003; data following heating above 1100 K excluded), Kung (unpublished) and Zhao et al. (1995); $\sigma(v/v_0) = 0.001$.

§§ G and $L(T)$ from Brillouin scattering measurements of $C_{ij}(T)$ by Jackson et al. (2007) and $M(T)$ ($T \leq 1125 \text{ K}$) from ultrasonic interferometry on the polycrystal of the present study; $\sigma(M)/M = 0.01$. Values of K_0 , G_0 , K'_0 , and G'_0 constrained as described in note **.

|||| As for note §§, but with values of K_0 , G_0 , K'_0 , and G'_0 constrained as described in note ††.

A comprehensive model for the thermoelasticity of MgSiO₃ orthoenstatite

Our experimental results, along with relevant data from the literature, have been assimilated into the thermodynamically consistent finite-strain (SLB) model of Stixrude and Lithgow-Bertelloni (2005). This approach and its application to ScAlO₃ perovskite have been outlined by Jackson and Kung (2008).

Premonitory softening of the elastic moduli of MgSiO₃ orthopyroxene is associated with its transformation to a high-temperature phase, as previously discussed. This suggestion is reinforced by the data of the present study (Fig. 4 and 5) and accordingly, all data acquired on heating beyond 1125 K and during subsequent cooling have been excluded from the fits reported in Table 3 and displayed in Figure 10 [the slightly higher temperature threshold for marked softening of the elastic moduli than for the earlier linear fits to v_s and $v_p(T)$ is justified by the fits of Fig. 10]. Even more pronounced softening of the elastic moduli in anticipation of the pressure-induced transition to the high-pressure clinoenstatite polymorph is evident in the data of Kung et al. (2004). We have therefore excluded from the fitting all data for $P > 8 \text{ GPa}$ at room temperature.

The data sets of Table 3, fitted sequentially and iteratively to the SLB model, serve to constrain the values of the model parameters highlighted in boldface. Thus the temperature-dependent entropy $S(T)$ derived from specific heat measurements provides the primary constraint on the value of the (initial) value θ_0 of the Debye temperature at ambient conditions. Likewise the K and $G(P)$ data best constrain K_{T0} , K'_{T0} , G_0 , and G'_0 , the $V(T,P)$ data the initial value γ_0 of the Grüneisen parameter, and the $L(T)$ and $G(T)$ data the values, respectively, q_0 and η_{S0} , of the initial logarithmic volume derivative and initial shear strain derivatives of γ . The variation of the third-law entropy S with temperature is somewhat over-predicted by the model (even with $\gamma_0 = 0$). We have therefore followed the approach of Stixrude and Lithgow-Bertelloni (2005) in using $S(1000 \text{ K})$ to constrain the preferred STP value of the effective Debye temperature θ_0 .

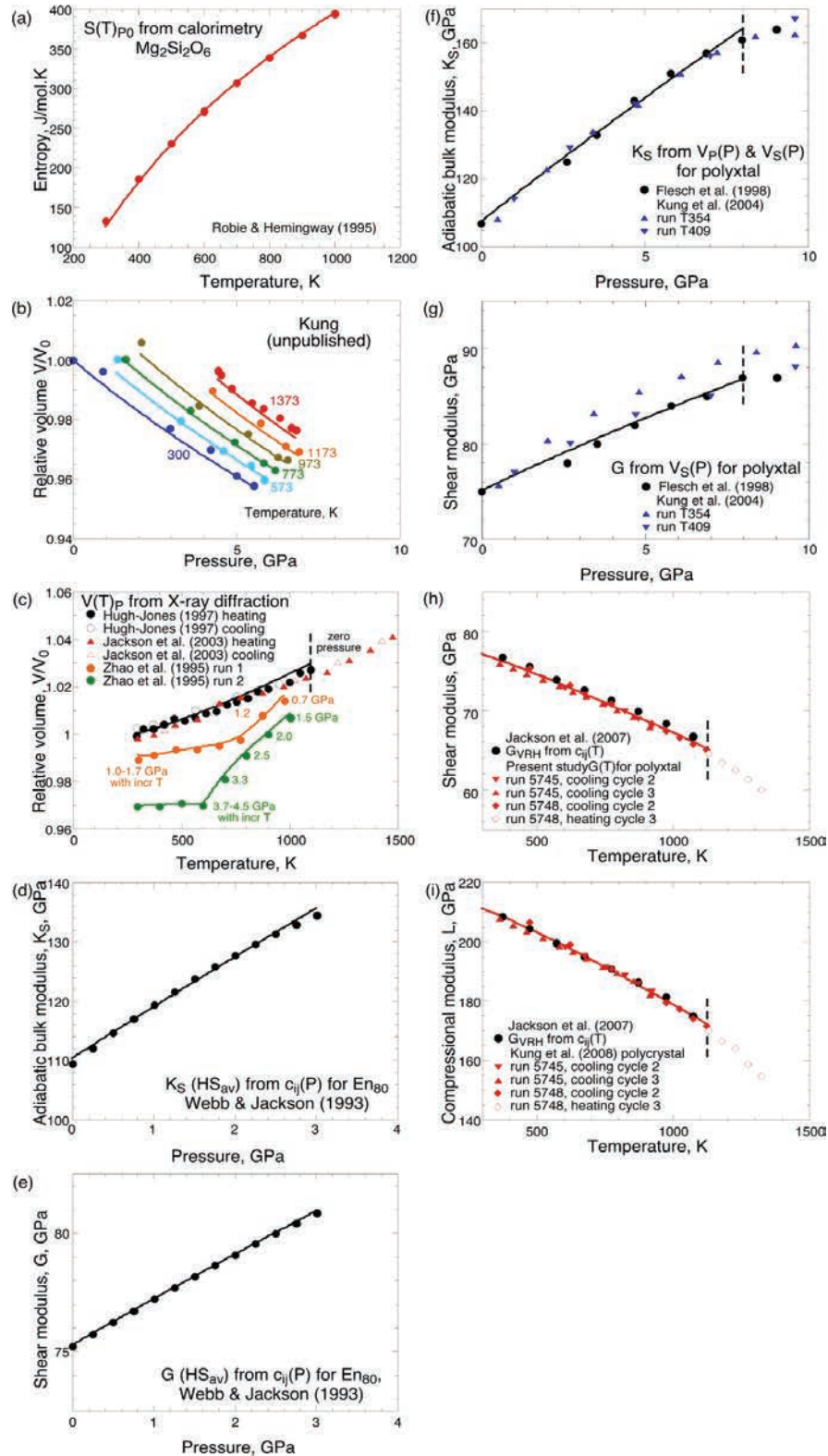


FIGURE 10. Comparison of thermoelasticity data for magnesian orthopyroxene with the preferred SLB model (Table 3—represented by the curves). Data obtained after heating beyond 1125 K at atmospheric pressure and compressing beyond 8 GPa at room temperature were excluded from the non-linear least-squares fits (see text for details). **(a)** Entropy. **(b** and **c)** P - V - T data (Kung, unpublished data; Zhao et al. 1995; Hugh-Jones 1997; Jackson et al. 2003). **(d–g)** Pressure dependence of the elastic moduli. **(h** and **i)** Temperature dependence of the elastic moduli.

Systematic misfit resulting in $(\chi^2/N)^{1/2} > 1$ (Table 3) is also associated with the fit of the model to precise single-crystal elasticity data for the En₈₀[(Mg_{0.8},Fe_{0.2})SiO₃] composition (Webb and Jackson 1993). The rate at which K' decreases with increasing pressure is substantially greater than allowed in the third-order Eulerian formulation in which the value of K''_{T0} is fixed by the requirement that $K_{T0}K''_{T0} = K'_{T0}(K'_{T0} - 7) - 143/9$. Similar behavior for the En₁₀₀ (MgSiO₃) composition may be masked by the lower precision of the data from solid-medium ultrasonic studies of polycrystals.

There remains significant uncertainty concerning the appropriate value of G'_0 . We tentatively prefer the value of 1.6(1) constrained by fitting the consistent data of Flesch et al. (1998) and Kung et al. (2004, run T409), but note that the value of 2.11(16) required by the data of Kung et al. (2004, Run T354) is closer to the well-constrained value of 1.98(2) for En₈₀. We note from Table 3 that the need to fit $G(T)$ with a mixture of intrinsic [$1/(\alpha G)(\partial G/\partial T)_V$] and extrinsic [$-(K_T/G)(\partial G/\partial P)_T$] contributions means that a higher value of G' (≈ 2.11) would inevitably be associated with a lower value of η_{80} (≈ 1.84).

Finally, we note that in fitting the $V/V_0(T,P)$ data set, there is some tension between the data sets describing thermal expansion at one-atmosphere and at high pressure. The preferred model is a compromise, tending to systematically overestimate the high-temperature (>900 K) volumes at one atmosphere and systematically underestimate the high-temperature volumes (>1100 K) at high pressure.

Data pertaining to room-temperature compression of MgSiO₃ orthoenstatite were not employed in our modeling of its thermoelastic behavior. However, analysis of those data, along with the ultrasonic data of Flesch et al. (1998) and the STP bulk and shear moduli from Brillouin spectroscopy (Jackson et al. 1999), by Angel and Jackson (2002) yielded values of $K_{T0} = 105.8(5)$ GPa and $K'_{T0} = 8.5(3)$ closely comparable with those of our preferred model (Table 3). Our preferred model differs from that of Stixrude and Lithgow-Bertelloni (2005) and the subsequent iteration by Xu et al. (2008) mainly by having a higher value of γ_0 and a much lower value of q_0 (Table 3). Evaluation of the preferred model of Table 3 allows separation of the intrinsic and extrinsic contributions to the temperature derivative of the modulus M ($M = K_T, K_S, G$) given by the first and second terms on the right-hand side of the equation $(\partial M/\partial T)_P = (\partial M/\partial T)_V - \alpha K_T(\partial M/\partial P)_T$.

It is evident from Table 4 that $(\partial K/\partial T)_P$ is dominated by the extrinsic component especially for K_S , whereas the intrinsic and extrinsic terms contribute sub-equally to $(\partial G/\partial T)_P$. Thus

TABLE 4. Intrinsic and extrinsic components of the temperature derivatives of the elastic moduli for MgSiO₃ orthopyroxene given by $(\partial M/\partial T)_P = (\partial M/\partial T)_V - \alpha K_T(\partial M/\partial P)_T$, evaluated from the preferred SLB model of Table 3 at the representative temperatures of 300 and 1000 K at $P = 0$

Modulus M	Intrinsic $(\partial M/\partial T)_V$ (GPa/K)	Extrinsic $-\alpha K_T(\partial M/\partial P)_T$ (GPa/K)	Total $(\partial M/\partial T)_P$ (GPa/K)
300 K			
K_T	-0.0039 (16%)	-0.0204	-0.0243
K_S	+0.0002 (-1%)	-0.0204	-0.0202
G	-0.0065 (60%)	-0.0044	-0.0109
1000 K			
K_T	-0.0037 (10%)	-0.0321	-0.0358
K_S	+0.0001 (0%)	-0.0316	-0.0315
G	-0.0087 (56%)	-0.0068	-0.0155

the unusually high values of $K' = (\partial K/\partial P)_T$ and $|\partial M/\partial T|_P$ for orthoenstatite are tightly linked through the dominance of the extrinsic part of the temperature derivative. Such behavior, appropriately described by the SLB model, provides a caution against the use of potentially inconsistent experimental data from different sources in the interpretation of seismological models for the Earth's interior. Instead as new data become available, it is essential that the full set of model parameters be readjusted to fit the various experimental/computational data sets.

ACKNOWLEDGMENTS

We thank C. Saint for technical support. This experimental work reported in this paper was performed while J. Kung was a postdoctoral research associate at Stony Brook. This research was supported by a NSF grant (INT 02-33849 and EAR 02-29704) to R.C. Liebermann and a grant (LX0348106) from the Australian Research Council to I. Jackson for a collaborative research program between Stony Brook University and the Australian National University and National Science Council (NSC) funding to Jennifer Kung, Jennifer M. Jackson, Dongzhou Zhang, and anonymous reviewer are thanked for their helpful reviews.

REFERENCES CITED

- Angel, R.J. and Jackson, J.M. (2002) Elasticity and equation of state of orthoenstatite, MgSiO₃. *American Mineralogist*, 87, 558–561.
- Brown, W.L. and Smith, J.V. (1963) High temperature X-ray studies on the polymorphism of MgSiO₃. *Zeitschrift für Kristallographie*, 118, 186–212.
- Flesch, L.M., Li, B.S., and Liebermann, R.C. (1998) Sound velocities of polycrystalline MgSiO₃-orthopyroxene to 10 GPa at room temperature. *American Mineralogist*, 83, 444–450.
- Frisillo, A.L. and Barsch, G.R. (1972) Measurement of single-crystal elastic constants of bronzite as a function of pressure and temperature. *Journal of Geophysical Research*, 77, 6360–6384.
- Gasparik, T. (1990) A Thermodynamic model for the enstatite-diopside join. *American Mineralogist*, 75, 1080–1091.
- Ghose, S., Schomaker, V., and McMullan, R.K. (1986) Enstatite, Mg₂Si₂O₆—A neutron-diffraction refinement of the crystal-structure and a rigid-body analysis of the thermal vibration. *Zeitschrift für Kristallographie*, 176, 159–175.
- Hugh-Jones, D. (1997) Thermal expansion of MgSiO₃ and FeSiO₃ ortho- and clinopyroxenes. *American Mineralogist*, 82, 689–696.
- Isaak, D.G., Anderson, O.L., Goto, T., and Suzuki, I. (1989) Elasticity of single-crystal forsterite measured to 1700 K. *Journal of Geophysical Research*, 94, 5895–5906.
- Isaak, D.G., Ohno, I., and Lee, P.C. (2006) The elastic constants of monoclinic single-crystal chrome-diopside to 1,300 K. *Physics and Chemistry of Minerals*, 32, 691–699.
- Ito, H., Mizutani, H., Ichinose, K., and Akimoto, S. (1977) Ultrasonic wave velocity measurements in solids under high pressure using solid pressure media. In M.H. Manghni and S. Akimoto, Eds., *High-Pressure Research: Applications in Geophysics*, p. 603. Academic Press, New York.
- Jackson, I. and Kung, J. (2008) Thermoelastic behaviour of silicate perovskites: Insights from new high-temperature ultrasonic data for ScAlO₃. *Physics of the Earth and Planetary Interiors*, 167, 195–204.
- Jackson, I. and Niesler, H. (1982) The elasticity of periclase to 3 GPa and some geophysical implications. In S. Akimoto and M.H. Manghni, Eds., *High-Pressure Research in Geophysics*, p. 113. Center for Academic Publications, Japan.
- Jackson, J.M., Sinogeikin, S.V., and Bass, J.D. (1999) Elasticity of MgSiO₃ orthoenstatite. *American Mineralogist*, 84, 677–680.
- Jackson, J.M., Palko, J.W., Andraut, D., Sinogeikin, S.V., Lakshtanov, D.L., Wang, J.Y., Bass, J.D., and Zha, C.S. (2003) Thermal expansion of natural orthoenstatite to 1473 K. *European Journal of Mineralogy*, 15, 469–473.
- Jackson, J.M., Sinogeikin, S.V., Carpenter, M.A., and Bass, J.D. (2004) Novel phase transition in orthoenstatite. *American Mineralogist*, 89, 239–244.
- Jackson, I., Webb, S., Weston, L., and Boness, D. (2005) Frequency dependence of elastic wave speeds at high temperature: a direct experimental demonstration. *Physics of the Earth and Planetary Interiors*, 148, 85–96.
- Jackson, J.M., Sinogeikin, S.V., and Bass, J.D. (2007) Sound velocities and single-crystal elasticity of orthoenstatite to 1073 K at ambient pressure. *Physics of the Earth and Planetary Interiors*, 161, 1–12.
- Jahn, S. (2008) High-pressure phase transitions in MgSiO₃ orthoenstatite studied by atomistic computer simulation. *American Mineralogist*, 93, 528–532.
- Jordan, T.H. (1978) Composition and development of continental tectosphere. *Nature*, 274, 544–548.
- Kung, J., Li, B.S., Uchida, T., Wang, Y.B., Neuville, D., and Liebermann, R.C. (2004) In situ measurements of sound velocities and densities across the orthopyroxene \rightarrow high-pressure clinopyroxene transition in MgSiO₃ at high pressure. *Physics of the Earth and Planetary Interiors*, 147, 27–44.

- Larson, A.C. and Von Dreele, R.B. (1988) GSAS Manual, Report LAUR 86-748. Los Alamos National Laboratory, Los Alamos, New Mexico.
- Le Bail, A., Duroy, H., and Fourquet, J.L. (1988) *Ab-initio* structure determination of LiSbWO₆ by X-ray-powder diffraction. *Materials Research Bulletin*, 23, 447–452.
- Lee, W.E. and Heuer, A.H. (1987) On the polymorphism of enstatite. *Journal of the American Ceramic Society*, 70, 349–360.
- McDonough, W.F. and Rudnick, R.L. (1998) Mineralogy and composition of the upper mantle. In R.J. Hemley, Ed., *Ultrahigh-pressure mineralogy: Physics and Chemistry of the Earth's Deep Interior*, vol. 37, p. 139–159. *Reviews in Mineralogy*, Mineralogical Society of America, Chantilly, Virginia.
- Murakami, T., Takeuchi, Y., and Yamanaka, T. (1982) The transition of orthoenstatite to protoenstatite and the structure at 1080 °C. *Zeitschrift für Kristallographie*, 160, 299–312.
- Niesler, H. and Jackson, I. (1989) Pressure derivatives of elastic wave velocities from ultrasonic interferometric measurements on jacketed polycrystals. *Journal of the Acoustical Society of America*, 86, 1573–1585.
- Ohashi, Y. (1984) Polysynthetically twinned structures of enstatite and wollastonite. *Physics and Chemistry of Minerals*, 10, 217–229.
- Ohi, S., Miyake, A., and Yashima, M. (2010) Stability field of the high-temperature orthorhombic phase in the enstatite-diopside system. *American Mineralogist*, 95, 1267–1275.
- Robie, R.A., Hemingway, B.S., and Bruce, S. (1995) Thermodynamic properties of minerals and related substances at 298.15K and 1 bar (10⁵ Pascals) pressure and at higher temperature. U.S. Geological Survey Bulletin, 2131, 461.
- Schrader, H., Boysen, H., Frey, F., and Convert, P. (1990) On the phase-transformation proto-ortho-enstatite to clino-ortho-enstatite—neutron powder investigation. *Physics and Chemistry of Minerals*, 17, 409–415.
- Shimobayashi, N. and Kitamura, M. (1993) Phase transition of orthoenstatite to high-clinoenstatite: in situ TEM study at high temperature. *Mineralogical Journal*, 16, 416–426.
- Smyth, J.R. (1974) Experimental study on polymorphism of enstatite. *American Mineralogist*, 59, 345–352.
- Stixrude, L. and Lithgow-Bertelloni, C. (2005) Thermodynamics of mantle minerals—I. Physical properties. *Geophysical Journal International*, 162, 610–632.
- Webb, S.L. and Jackson, I. (1993) The pressure-dependence of the elastic-moduli of single-crystal ortho-pyroxene (Mg_{0.8}Fe_{0.2})SiO₃. *European Journal of Mineralogy*, 5, 1111–1119.
- Xu, W.B., Lithgow-Bertelloni, C., Stixrude, L., and Ritsema, J. (2008) The effect of bulk composition and temperature on mantle seismic structure. *Earth and Planetary Science Letters*, 275, 70–79.
- Yang, H.X. and Ghose, S. (1994) Thermal-expansion, Debye temperature and Grüneisen-parameter of synthetic (Fe, Mg)SiO₃ orthopyroxenes. *Physics and Chemistry of Minerals*, 20, 575–586.
- (1995) High-temperature single-crystal X-ray-diffraction studies of the ortho-proto phase-transition in enstatite, Mg₂Si₂O₆ at 1360 K. *Physics and Chemistry of Minerals*, 22, 300–310.
- Zhao, Y.S., Schiferl, D., and Shankland, T.J. (1995) A high *P-T* single-crystal X-ray-diffraction study of thermoelasticity of MgSiO₃ orthoenstatite. *Physics and Chemistry of Minerals*, 22, 393–398.
- Zucker, R. and Shim, S.H. (2009) In situ Raman spectroscopy of MgSiO₃ enstatite up to 1550 K. *American Mineralogist*, 94, 1638–1646.

MANUSCRIPT RECEIVED JUNE 13, 2010
MANUSCRIPT ACCEPTED NOVEMBER 6, 2010
MANUSCRIPT HANDLED BY WENDY MAO